OVERVIEW OF THE RF BASED BEAM DIAGNOSTIC MONITORS OF HIPA AT PSI

J. Sun†, P.-A. Duperrex, PSI Center for Accelerator Science and Engineering, Villigen, Switzerland

Abstract

The High Intensity Proton Accelerator (HIPA) at the Paul Scherrer Institute (PSI) delivers a continuous-wave (CW) proton beam at a frequency of 50.63 MHz, with currents up to 2.2 mA and a maximum energy of 590 MeV. The beam is successively directed to two meson production targets before reaching the spallation target. To monitor key beam parameters, various diagnostics based on the RF beam signal detection have been implemented. For beam intensity and energy measurements, resonators tuned at the second harmonic (101.26 MHz) have been deployed on the different beam lines. Capacitive probes in the cyclotrons provide the phase measurements. In addition, a cross-correlation technique applied to phase pick-up signals at the entry and exit of the cyclotron, enables a precise determination of the number of turns completed by the beam. Beam alignment on a rotating target is monitored using a novel fin-and-groove structure engraved on the target surface. The resulting intensity modulation, measured with a downstream beam current monitor, is analysed in the frequency domain to directly infer the beam offset on target. More details are described below.

INTRODUCTION

The HIPA can generate up to 1.4 MW continuous proton beam, the proton beam is accelerated from a Cockcroft-Walton source followed by two cyclotrons: the so-called Injector 2 cyclotron accelerating the beam from 870 keV to 72 MeV and the so-called Ring cyclotron accelerating it to 590 MeV. The beam is then directed through 2 meson graphite targets (Target M and E) to the spallation neutron source SINQ [1]. The Target M has a thickness of 5 mm and absorbs ~1% of the beam. The Target E is 40 mm (alternatively 60 mm) thick and absorbs ~8% (~12%) of protons, layout of the whole facility can be found in Fig. 1. An upgrade project called IMPACT (Isotope and Muon Production using Advanced Cyclotron and Target technologies) is ongoing aiming to renew the Target M and related muon beam lines and build up an online isotope separation facility [2].

Many beam diagnostics monitors that are based on RF signal detection were designed for beam development and operation, a schematic plot can be found in Fig. 2. Resonator type beam current monitor is a key element for beam intensity and transmission measurement, which is also integrated into the interlock system to protect the machine from the abnormal beam jitters or too high beam losses. Inductive pickups are used for bunch phase detection for the two cyclotrons and can be further served as number of turn measurement. For the beam off-axis detection, grooves and bumps are manufactured on the target E, beam intensity then is modulated, and the off-axis information can be derived from the amplitude difference between the specific modulated signals of the downstream current monitor.

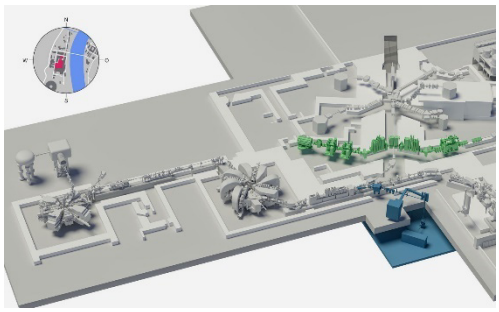

Figure 1: Layout of HIPA with upgrade project IMPACT.

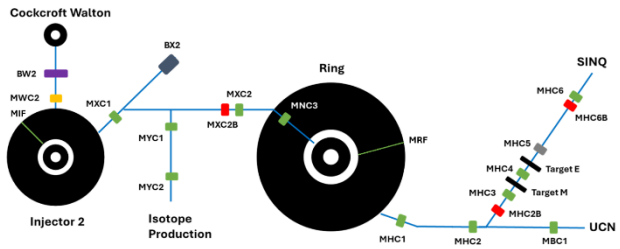

Figure 2: Schematic of the RF based monitors of HIPA, M*F indicates the phase monitors and M*C indicates the current monitors.

RESONATORS

Coaxial resonator (reentrant cavity) [3] can be tuned to a specific resonance frequency by modifying the dimension of the capacitance gap and the inductance wall, see Fig. 3 left. A wall current with the same time structure as the beam bunch will be induced when the bunch passes through the cavity. The amplitude of the magnetic field, as shown in Fig. 3 right, in the resonator is directly proportional to the beam current, a measurement of this field provides a measure of the beam intensity.

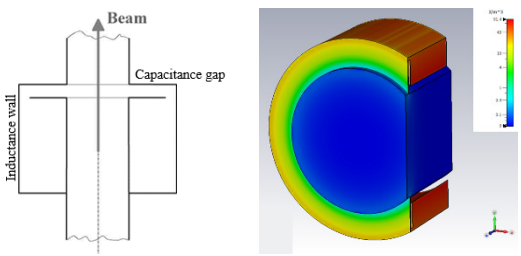

Figure 3: Principle sketch of the cavity type monitor (left); Magnetic field distribution in the cavity (Right).

† jilei.sun@psi.ch

Beam Intensity Measurement

At PSI, the coaxial resonator is tuned at the 2nd harmonic (101.26 MHz) of the HIPA bunch frequency. Second harmonics are used because of the better signal-to-noise ratio, the RF disturbance components being mainly at the odd harmonics. The beam intensity measurement system consists of many beam current monitors mounted on the different beam transport lines for intensity measurement and transmission calculation; the overall layout can be found in Fig. 2.

Beside the coaxial resonators, there are also 3 Bergoz current monitors, which measure the current in absolute way, running as a reference for the other beam current monitors. In addition, beam dump e.g., BX2 can also provide absolute beam intensity value for calibration.

The signal from the monitor is brought to the electronics by using low-loss 50-Ohm cables, with lengths between 50 and 250 m. The output is further used for the transmission calculation and interlock generation when the current value is above a given limit.

MHC5

A special beam intensity monitor, so called MHC5, is located 8 meters downstream of target E in the high-energy beam line, can be seen in Fig. 2. MHC5 is a key element for beam operation, as any deviation from the expected transmission from target E could damage the spallation target SINQ.

The main concern for MHC5 is the energy deposition from the scattered particle shower due to the target E. This causes large temperature variations in the resonator, leading to resonance frequency and calibration drifts during operation. To address this issue, an aluminum cavity with active cooling was first implemented. However, the resonance frequency shift was still too large. A later study showed that the cavity thermal gradient due to active cooling was inducing an even larger shift [3]. Therefore, materials with lower thermal expansion coefficients and higher radiation emissivity (since the resonator is in the beam line vacuum) were considered for a new MHC5 design.

Graphite has several advantages over aluminum for the MHC5 cavity, lower thermal expansion coefficient reduces thermal deformation, leading to smaller frequency drift, higher radiation emissivity improves cooling and reduces temperature excursions. Without active cooling, thermal gradient issues are minimized. Additionally, its lower electrical conductivity reduces the cavity's Q factor, making the resonator less sensitive to frequency drift. Further simulation studies show that thermal expansion always causes negative frequency drift, which means higher temperature leading to a lower resonance frequency. One possible way to counteract this effect is to use a second material with a much larger expansion coefficient to increase the capacitor gap, thereby increasing the resonance frequency. This self-compensating method was implemented by inserting a thin aluminium shim at the capacitor gap position, as shown in Fig. 4. The first graphite monitor was installed into the beam line in early 2015.

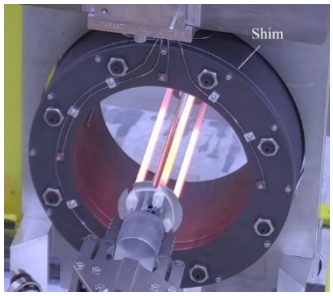

Figure 4: The graphite MHC5 being tested after maintenance in 2017, quartz tube in the center of the monitor to simulate the thermal load effects on the resonator.

An upgrade design for MHC5 was finished in 2023 with many features [4]. From the maintenance perspective, MHC5 is operating in an extremely high radiation area, hanging under a 2.5 m long bulky steel shielding in the beam bunker. In the past, the whole shield had to be replaced for a new resonator installation. To minimize the radioactive wastes, the new modular design (see Fig. 5 left) allows the upper segments to be re-used in case of monitor failure. To minimize the human exposure to radiations in case of repairs or maintenance, a PSI solution was specially developed for the cable plugin/out to the pickups allowing the use of manipulators (Fig. 5 middle).

Grooves with 5 mm radius and 100 mm length were milled at the inner surface of the previous design of MHC5, to mount 4 inductive pick-ups providing an additional BPM measurements capability. The new design incorporates a major improvement by increasing the number of pickups to eight and with capacitive pickups, or buttons. This enhancement will improve not only the intensity and position measurements but will also provide an ellipticity estimate, in addition, the possibility to measure the bunch length. The shorter pickups have a better time domain response.

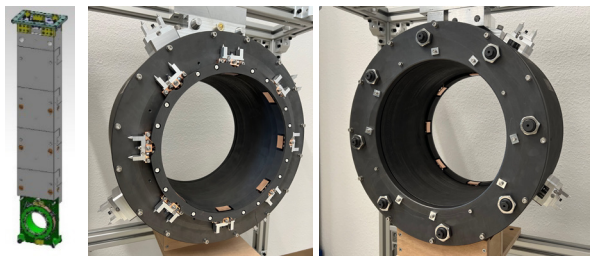

Figure 5: Overview of the improvement design of the MHC5 and its shielding (left); Details of the new MHC5 with 8 BPM buttons and the remote plugin/out structure (middle and right).

Beam Energy Measurement

The old CAMAC based electronics have served for decades for beam intensity measurement. A new VME based version has been developed to replace the CAMAC. The VME system provides not only amplitude of the 101.26 MHz signal but also phase information. This enables the extraction of the beam energy through the time-of-flight (TOF) method, by employing a pair of current monitors along the beam line, such as MXC1 and MXC2. The same

approach can also be applied to the high-energy beam transport line downstream of the Ring [5].

There are two phase delays to be considered during the calculation, cable delay and electronic delay. The cable phase delay can be easily calculated out by measuring the cable length. The phase delay of each electronics channel cannot be determined, but the phase difference between two channels can be approached by swapping the input signals at the input ports of the electronics.

Assuming φ_1 and φ_2 are the measured phase value from two current monitors.

$$\varphi_1 = \varphi_{I1} + \varphi_{D1}$$

$$\varphi_2 = \varphi_{I2} + \varphi_{D2}$$

where φ_{I1} and φ_{I2} are the phase at the input ports of each electronic channels, φ_{D1} and φ_{D2} are the phase delay caused by the electronics. The phase difference between these two current monitors shows as follows:

$$\varphi_2 - \varphi_1 = \varphi_{I2} - \varphi_{I1} + \Delta_\varphi \quad (1)$$

where $\Delta_\varphi = \varphi_{D2} - \varphi_{D1}$ is the phase difference between electronic channels. After swapping the cables at the input ports of the electronics, one can have:

$$\varphi_2 - \varphi_1 = \varphi_{I1} - \varphi_{I2} + \Delta_\varphi \quad (2)$$

Then the phase difference between electronic channels can be calculated out:

$$\Delta_\varphi = \frac{(1) + (2)}{2}$$

The measured beam energy after Injctor2 with respect to the beam intensity can be found in Fig. 6, the accuracy of the measurement is better than 1%.

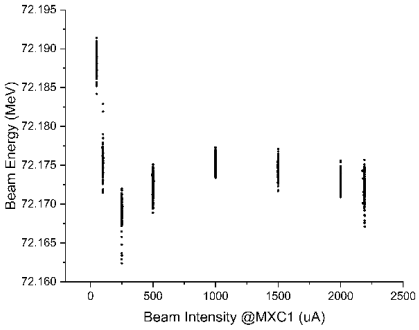

Figure 6: Injector 2 beam energy measured under different beam intensity.

CAPACITIVE PHASE PROBES

One of the crucial parameters to be set correctly while tuning HIPA is the number of turns in the cyclotrons; this parameter can change after a long maintenance period.

In the past, the number of turns for HIPA had to be measured using radial probes. A handicap of such measurements is that it can be performed only during dedicated beam development time. An on-line estimate of the number of turns during normal operation is then developed based on the acceleration voltage measurements, with the 1-2% inherent limited precision of RF measurements. A new scheme based on the Time of Flight (ToF) measurements has been developed to remove the limitations of the previous techniques. Normally the ToF is deduced by comparing the fast sampled signals from capacitive pickups at the entrance and exit of each cyclotron, an overview of the radially arranged pickups of the Ring cyclotron is shown in Fig. 7.

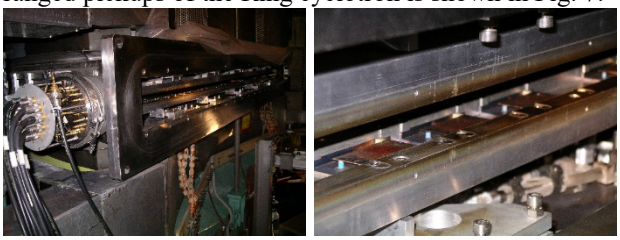

Figure 7: Radially arranged capacitive pickups in the Ring cyclotron.

Capacitive pickups are usually dedicated to the phase measurements in the cyclotrons. The pickup signals have been recorded using a Compact PCI based ADC board with 3 GHz sampling rate and 12-bit resolution. The signal processing consists first of the envelope detection of each capacitive pickup signal before cross-correlating. The delay corresponding to the cross-correlation maximum provides then an estimate of the ToF. Without the envelope pre-processing, the cross-correlation on the raw data would just deliver maxima at time differences corresponding to the repetition rate of the pulses (~50.6 MHz) [6].

Number of Turn Determination

The number of turns is the ratio between the effective time spent by a proton bunch in the cyclotron $T_{cyclotron}$ and T_{rev} , the time for a proton bunch to perform one revolution:

$$n_{turn} = {T_{cyclotron}}/{T_{rev}}$$

The revolution time T_{rev} is given by:

$$T_{rev} = {h}/{f_{RF}}$$

where h being the harmonic number, i.e. the number of bunches on a given turn. For the Ring, h is 6 and for the Inj.2 is 10, with respectively a time needed for one turn of 118.7 ns and 197.5 ns.

$T_{cyclotron}$ is obtained from the measured time delay with a correction ΔT_{cable} due to the length difference of the cables used for the measurements. An additional correction Δn_{pickup} is needed to compensate the position of the pickups which differ from the exact entrance and exit of the cyclotron.

$$n_{turn} = \frac{(T_{ToF} - \Delta T_{cable}) \cdot f_{RF}}{h} - \Delta n_{pickup}$$

Signal Processing and Time Delay Measurements

Waveforms up to 1 ms long were recorded with the ADC board. These waveforms were then can be analyzed either on-line with the higher-level program or off-line by using MATLAB. Fig. 8 shows an off-line number of turn measurements of Inj.2. Upper plot shows the raw data from two pickups that before and after the Inj.2, lower shows the result of the cross-correlation of the envelopes from the raw

data, where we can have T_{ToF} is 11.71 µs. With the corrections of ΔT_{cable} = -50 ns and $\Delta n_{pickup} \approx$ 1:

$$n_{turn} = \frac{(11.712 \cdot 10^{-6} + 5.0 \cdot 10^{-8}) \cdot 50.633 \cdot 10^{6}}{10} - 1 \approx 59$$

which is consistent with the standard measurements using the radial probes.

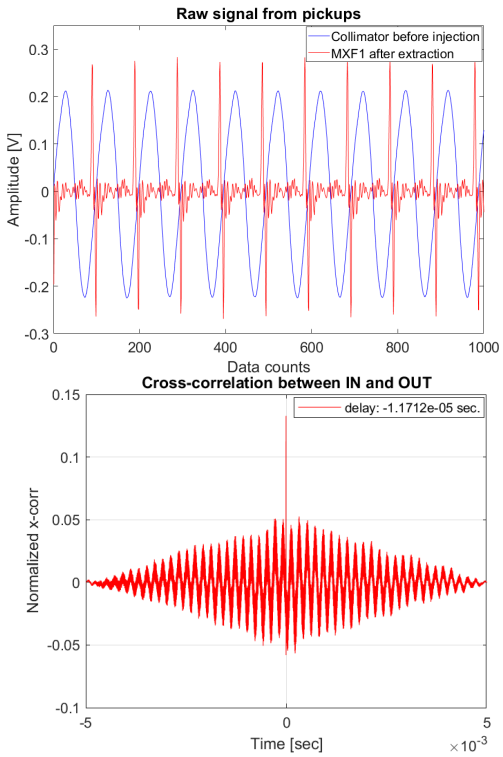

Figure 8: Raw signal from two pickups that before and after the Inj.2 (upper), result of the cross-correlation of the envelopes from the raw data (lower), the peak shows the ToF of the bunch between these two pickups.

BEAM ON TARGET DETECTION

Target E, as shown in Fig. 2, is a key component for experiments of nuclear and material research, which is rotating in 1 Hz. Centring the beam on the target is an important task for the operation and has safety issues in case of beam misalignment. The correct centring of the beam on the Target E is important since the rim of the wheel is only 6 mm wide. Missing partly the target would not only reduce the meson production rate but also leads to a pencil beam hitting the SINQ target window, which could not withstand such power densities.

Transmission minimization is the standard method to centre the beam position on the Target. The transmission is the ratio of the beam current measured after and before the target. For this method, a beam position scan is performed to identify the range and the optimum position corresponding to the minimum transmission. This is however an indirect measurement and is not very sensitive.

The new developed method allows a more sensitive detection of off-axis beam conditions, schematic can be found in Fig. 9. The method is based on the detection of beam current (MHC5) modulations induced by grooves and protrudes manufactured on the target rim. Evidence of these modulations is indicative of off-axis beam conditions, the modulation amplitude giving some information about how far off-axis the beam is located. For testing, the relative position of the beam on the target can be controlled by a set of steering magnets in the range of -1.3 mm to 1.3 mm. The beam current signals are recorded using a 16-bit data logger at a 10 kHz sampling frequency. LabVIEW was used to remotely control the data logger, perform the modulation detection and to configure an EPICS server for easy access to the results [7].

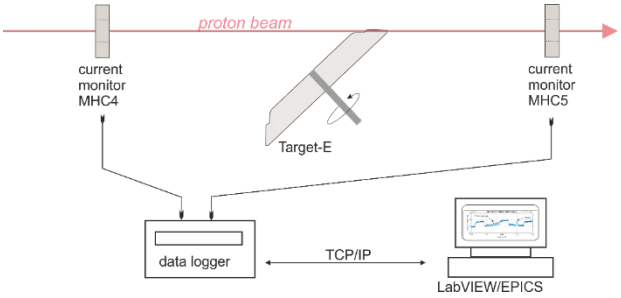

Figure 9: Schematic of the beam on target detection.

Grooved Target

The first version of Target E for this experiment is shown in Fig. 10. The tests took place in the summer 2019 for 2 months, the target then had to be replaced due to bearing problems. The target is divided into 12 segments. Between the segments a 1 mm wide gap allows for thermal expansions as well as dimensional changes due to irradiation.

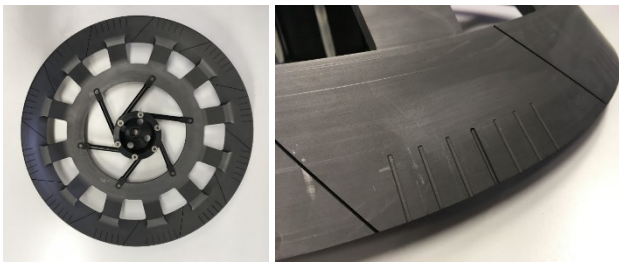

Figure 10: The Target E used for testing. Detail of a segment showing the grooves. On the particular segment the middle groove is milled 1 mm deep (the other grooves of this segment are 0.3 mm deep). This groove acts as absolute marker.

The grooves on each segment can be easily visible in Fig. 10. The spaces between each groove have been calculated so that, for a target rotating at 1 Hz, a beam current modulation on MHC5 at either 114 Hz (left off-axis) or 138 Hz (right off-axis) will be measured. These two frequencies have been chosen so that they are located exactly between two harmonics of the 12 Hz signal generated from the target blades.

4 groove milling depths were tested on this target: 0.3, 0.5, 0.7 and 0.9 mm on groups of 3 elements distributed equally to investigate the sensitivity of the detection and the possible physical defects. One groove on each side was milled deeper (1 mm) to act as an absolute marker (see Fig. 10).

Signal Processing

To detect the groove modulation on the MHC5 signal, it was necessary to filter the broadband noise already present on the signal. The MHC4 signal was used for that purpose. By subtracting the correctly weighted MHC4 signal from the MHC5 one, most of the noise contributions prior to the Target E can be removed. The 12 Hz modulation from the blades are easily visible as well as a 1 Hz rotation wobbling.

The FFT of the filtered MHC5 is then performed to detect the possible presence of the 114 Hz or 138 Hz spectral lines, as well as their corresponding harmonics.

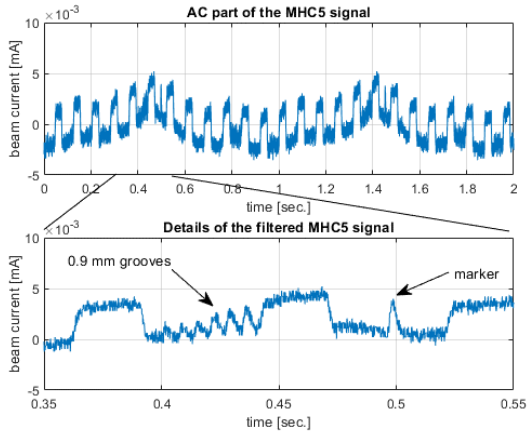

Figure 11: Example of modulations for off-axis position.

An example of the data for +1.3mm beam offset at beam intensity of 0.388 mA shows in Fig. 11. The beam intensity modulation due to the absolute marker on the first segment is clearly visible as well as the 138 Hz 0.9 mm groove effects.

The groove modulation level dependency on the off-axis beam position has been analysed for 1.6 mA beam intensity conditions. For this study, the beam position on the target has been changed from -1.3 to +1.3 mm with 0.1 mm increment. The 114 Hz and 138 Hz spectral line amplitudes have been measured for each position using the FFT routine and the results are shown in Fig. 12 up.

For centred beam conditions, no spectral lines at 114 Hz and 138 Hz are detected the noise level. For off-axis distance larger than 0.7mm the spectral lines have been clearly detected. The non-linear dependency stems from the shape and profile of the beam.

To compare the performance of the new method with the transmission measurements, the transmission level as function of the beam position is shown in Fig. 12 down. The transmission is clearly much less sensitive compared to the groove modulation detection.

New Configuration of the new Target

Based on the experiences collected in the last years, a new configuration has been applied on the new Target E. Grooves and protrudes are both manufactured, where grooves indicate the beam in the centre and protrudes indicate the beam is off axis to the left or right, details can be found in Fig. 13.

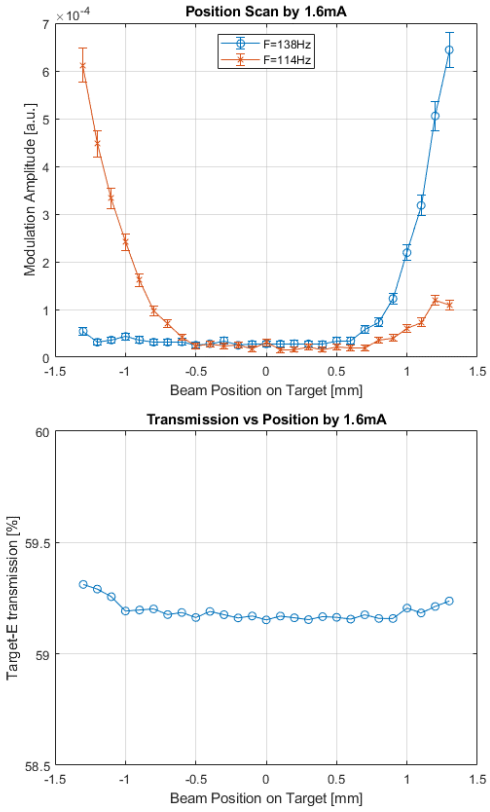

Figure 12: 114 Hz and 138 Hz spectral lines as function of the beam position on the target (up); Transmission as function of the beam position (down).

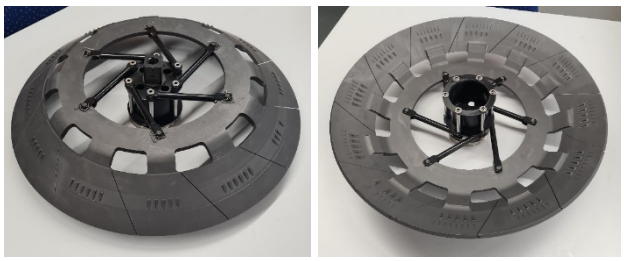

Figure 13: New configuration of the target.

CONCLUSION

Monitors based on RF signal detection are key components of the beam diagnostics system of HIPA at PSI. Resonator type monitors provide not only beam intensity but also used for transmission calculation for machine protection. Thanks to the newly developed electronics beam energy now can also be derived from the resonator signal, which is very helpful for the machine setup and operation, especially for isotope production. Number of turn measurements based on the phase probe signal and the beam off axis detection on Target E are new developments in the last years, which also play an important role during setup and machine study.

REFERENCES

[1] D. Kiselev *et al*., "The meson target stations and the high power spallation neutron source SINQ at PSI," *J. Radioanal. Nucl. Chem.*, vol. 305, no. 3, pp. 769–775, Feb. 2015. doi:10.1007/s10967-015-3999-3

[2] D. Kiselev *et al*., "IMPACT: a substantial upgrade to the HIPA infrastructure at PSI", in *Proc. Cyclotrons'22*, Beijing, China, December 2022, pp. 34-37. doi:10.18429/JACoW-CYCLOTRONS2022-MOBO02

[3] J. Sun *et al*., "Design of a new beam current monitor under heavy heat load", in *Proc. HB'14*, East Lansing, USA, November 2014, pp. 154-156.

[4] P.-A. Duperrex *et al*., "Improvement design of a beam current monitor based on a passive cavity under heavy heat load and radiation", in *Proc. HB'23*, Geneva, Switzerland, October 2023, pp. 205-209. doi:10.18429/JACoW-HB2023-WEC1C1

[5] J. Sun *et al*., "Optimization of beam intensity measurement system of HIPA at PSI", in *Proc. IBIC'25*, Liverpool, UK, September 2025, pp. 200-203. doi:10.18429/JACoW-IBIC2025-MOPMO12

[6] P.-A. Duperrex and A. Facchetti, "Number of turn measurements on the HIPA cyclotrons at PSI", in *Proc. IPAC'18*, Vancouver, Canada, April-May 2018, pp. 2334-2336. doi:10.18429/JACoW-IPAC2018-WEPAL067

[7] P.-A. Duperrex *et al*., "New centring beam monitor for high power proton beam rotating target", in *Proc. Cyclotrons'19*, Cape Town, South Africa, September 2019, pp. 189-191. doi:10.18429/JACoW-Cyclotrons2019-TUP016